applied sciences

MDPI

Article

Reduction of Satellite Signature Effect in High-Accuracy Satellite Laser Ranging to Etalon

Ning An [1,*], Bowen Guan [1], Natalia Edith Nunez [2], Jian Gao [1], Xue Dong [1], Haitao Zhang [1] and Ricardo Cesar Podesta [3]

[1] Changchun Observatory, National Astronomical Observatories, Chinese Academy of Sciences, Changchun 130117, China
[2] Department of Astronomical Sciences, National University of San Juan, San Juan 5400, Argentina
[3] Felix Aguilar Astronomical Observatory (OAFA), San Juan 5400, Argentina
* Correspondence: ann@cho.ac.cn; Tel.: +86-13756477783

Abstract: Etalon is considered to be one of the most promising satellites for studying crustal motions, Earth rotation, and other scientific applications. Unfortunately, its outsized shape and signature result in a measurement range bias of several millimeters. On the basis of simulations of the echo signals, we analyze the center of mass corrections (CoM) for Etalon due to variations in satellite signature effect at different incidence angles. To minimize range bias caused by satellite signature effects, a center of mass corrections filter has been proposed for the processing of standard SLR data. According to the relationship between RMS of CoM and the upper limits of the rejection criteria, the measurements with the lowest variability of CoM are selected for normal points. Statistics indicate that the center of mass corrections filter can improve the stability of the collected data by 79%, and reduce the mean RMS of normal points from 163.7 × 41.8 ps to 118.2 × 8.94 ps. Additionally, the new algorithm is applicable to Etalon-2. In particular, this paper enriches and provides a useful reference for minimizing the effects of satellite signatures on the production of SLR data by providing a theoretical model that incorporates systematic errors in SLR.

Keywords: satellite laser ranging; satellite signature effect; pro-processing algorithm; center of mass corrections; Etalon

check for updates

Citation: An, N.; Guan, B.; Nunez, N.E.; Gao, J.; Dong, X.; Zhang, H.; Podesta, R.C. Reduction of Satellite Signature Effect in High-Accuracy Satellite Laser Ranging to Etalon. *Appl. Sci.* **2023**, *13*, 11106. https://doi.org/10.3390/app131911106

Academic Editor: Zhengjun Liu

Received: 31 August 2023
Revised: 25 September 2023
Accepted: 30 September 2023
Published: 9 October 2023

1. Introduction

Ever since Etalon was launched in 1989, it has been dedicated to satellite laser ranging to support various scientific applications [1]. Observation data from Etalon are useful for analyzing the accuracy of terrestrial reference frames, modeling long-term disturbances, and conducting other geophysical studies [2]. As compared to LAGEOS satellite, Etalon satellite has a much higher orbit and is less affected by atmospheric drag. The variations in Earth's harmonic term at the orbital intersection are about one tenth of those observed by LAGEOS, which implies that Etalon might provide more reliable data for geodynamic research and analysis [3].

KHz satellite laser ranging has led to the flourishing application of research for Etalon satellites [4]. The new set of measurements presents new challenges for the post-processing of range measurements, as well as providing additional insights into the sources of potential errors. Satellite signature effect is one of the main sources of error in satellite laser ranging, which results in biases ranging from millimeters to centimeters [5,6]. Various pro-processing strategies have been developed to reduce the satellite signature effect on SLR products. In 2008, Kirhner et al. selected only the leading range measurements of LAGEOS-1/2 to improve the accuracy of normal points less than one millimeter [7]. In 2015, Kucharski and colleagues introduced the concept of the leading range filter, which retains only 10% of the overall range residuals as useful echo signals [8]. In 2017, Wilkinson proposed the use of tight clipping to improve the quality of LAGEOS observation data [9]. Prior algorithms attempted to minimize the satellite signature effect by modifying the acceptable return level according to empirical formulas or mathematical analysis with fixed values for center of mass corrections. Unfortunately, these methods fail to take into account the variations in satellite signature effects on the various reflections. As a result, range bias due to variations in the center of mass corrections cannot be eliminated.

In this paper, we simulate the reflected signals from Etalon and calculate the variations of the center of mass corrections at different incident angles on the basis of structural analysis. A quantitative assessment of the association between rejection criteria for returns and RMS of center of mass corrections is performed by taking into account the residual bias caused by variations in center of mass corrections. The normal point algorithm is then modified to incorporate a center of mass correction filter to minimize the effect of satellite signatures on the post-fitting range residual distributions. In this new algorithm, we intend to reduce the variability inherent in long arcs of observation data, and improve the stability and accuracy of the results obtained from these observations.

2. Satellite Signature Effect

Satellite laser ranging measures the distance between the telescope reference point of the terrestrial observatory and the center of mass of a satellite equipped with multiple retroreflectors. It is ideal for a satellite to have a spherical shape and to behave as an optical point-of-light target. However, Etalon is a highly dense spherical satellite in reality. It consists of 12 segments that are connected via welding on both the internal and external surfaces. A titanium and aluminum body composes Etalon satellite (diameter 1.294 m, weight 1415 kg). It has a hollow spherical shape and a wall thickness of 100 mm. A total of six germanium and 2140 fused-quartz corner cube reflectors of the same dimensions make up the array of retroreflectors. The positions of the corner cube reflectors on Etalon area units are shown in Figure 1 [10].

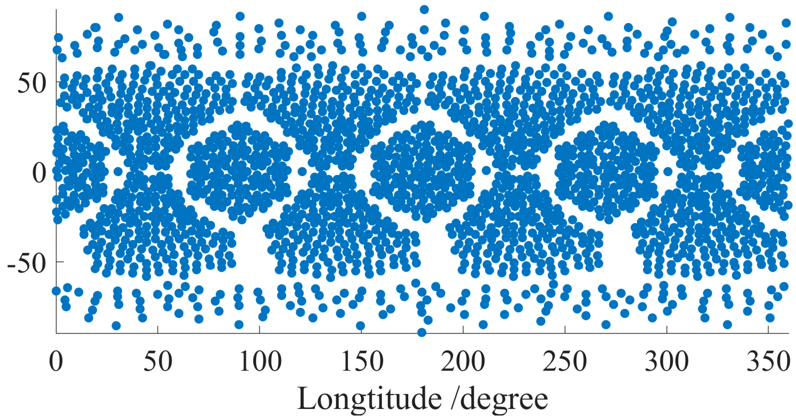

Figure 1. Arrangement of corner cube reflectors installed on the surface of Etalon.

It can be seen that the distribution of arrays on Etalon satellite is not homogeneous. Retro-reflectors are positioned in every bracket with a large distance between them. Based upon the geometrical characteristics of Etalon satellite, we can deduce the contribution of each retroreflector to the range measurement by using the retroreflector uneven distribution model [11]:

$$P_i(t) = n_i \times S_i \times I(t), \tag{1}$$

where n_i is the reflectance of the retroreflector, S_i is the reflection area, and $I(t)$ is the incident beam. The relative time delay ΔR_{delay} of each retroreflector can be written as [12]:

$$\Delta R_{delay} = R \times \cos\theta_i - L \times \sqrt{n_i^2 - \sin^2\theta}, \tag{2}$$

where R represents the radius from the satellite center to the surface of cube corner and θ_i is the angle between the normal of the retroreflector and the incident beam. Equations (1) and (2) indicate that the contribution of each retroreflector participated to the reflection is different. The response $P_r(t)$ of Etalon can be obtained by summing up these individual returns with neglecting the interference between the return signals.

$$P_r(t) = \sum_{i=1}^{k} P_i(t), \tag{3}$$

The final signal $P(t)$ received by the SLR system is obtained with the convolution of the system errors and the model of SPAD [12]:

$$P(t) = P_r(t) \otimes P_e(t) \otimes P_j(t), \tag{4}$$

where $P_e(t)$ is the SLR system error function and $P_j(t)$ is the time jitter or the SPAD in SLR system.

Figure 2 illustrates how the brightness of each retroreflector on Etalon satellite varies with different laser incident angles. The reflected signals from the nearer reflectors are stronger and arrive earlier than those from the farther ones. Reflector illumination patterns vary according to the angle of the incident laser. A recent report has found that the retroreflector area on Etalon is affected by the incident angles [13]. Consequently, the geometrical parameters of the retroreflectors on Etalon are supposed to be responsible for the apparent difference in reflected energy density. Further, the inhomogeneous retroreflector distribution (some space must be allocated to the holders and retroreflector separation) is a possible factor causing the serious satellite signature effect.

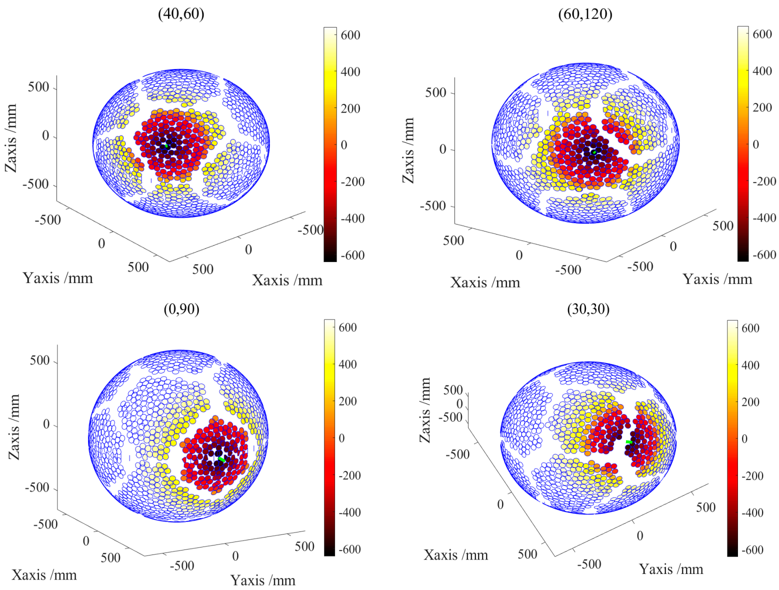

Figure 2. Distribution of laser reflection intensity of Etalon satellite angular reflector in different incident directions.

We simulate the response of Etalon satellite by using different incident angles, as shown in Figure 3. Variations in retro segments participating in the reflection result in different distributions of echo signals, as can be seen from the graph. It is apparent that Etalon's return signal distribution is significantly skewed towards shorter ranges with a long tail. There are still several reflections occurring at distances of up to 250 mm from the peak of the distribution. The waveform produced by the observations has been deformed and widened, and it exhibits multiple peaks at certain angles of incidence.

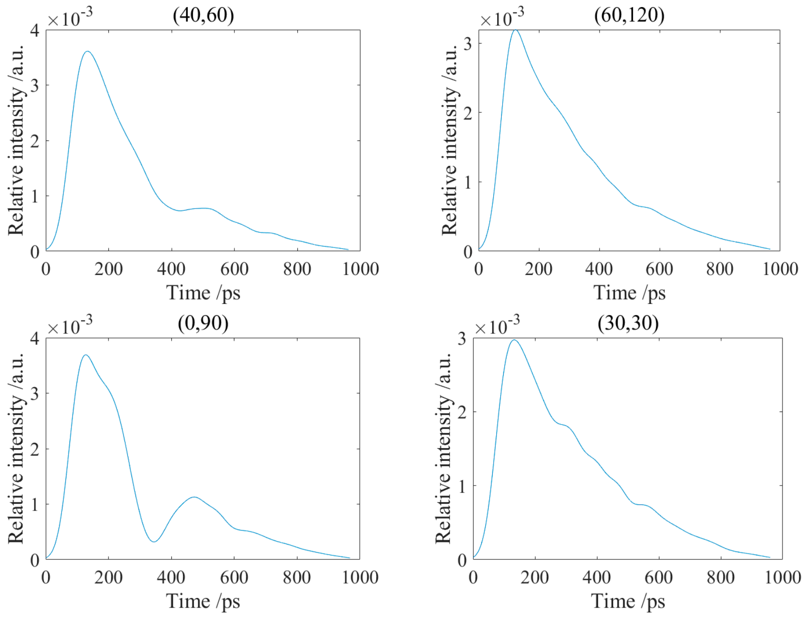

Figure 3. Distribution of the returned signals from Etalon at different incident angles.

For the purpose of testing the hypotheses described above, the SLR system in the Changchun observation was used to obtain observation data of Etalon. According to Appendix A, the working process of the SLR system at the Changchun station is as follows: Firstly, the azimuth, altitude, and distance of the target satellite in the station coordinate system are calculated using Etalon's prediction ephemeris. The telescope is guided by the control system to track the target in real time when the elevation angle of Etalon is greater than 20° relative to the Changchun station. Following the stabilization of the tracking, a laser pulse is emitted to the target satellite. Meanwhile, the laser pulse signal is transmitted by PIN to the constant ratio discriminator in order to record the transmission time. Upon receiving the echo signal from Etalon, a photodiode in the receiving system converts it into an electrical signal. By comparing the difference between the two moments of the event timer, we can determine the distance from the target satellite to the station.

Figure 4 indicates the statistical results of the residual distributions for Etalon in January 2021, while the orange curve represents the simulated echo signal based on the retroreflector uneven distribution model. In the case of raw observation data, the full rate residual histogram contains all the reflected signals from each incident direction during a typical period of segment tracking of 20 min. To obtain the average reflected pulse shape, we simulate reflected signals from 2594 incident directions equally distributed around Etalon and sum the displacements of individual pulses. The results presented in Figure 4 are consistent with the observed distribution of residuals, including the long tail. Pearson coefficient between simulated and experimental echo waveforms is 0.92, indicating that the spreading and deformation of the residual segments are caused by the accumulation of satellite signature effects.

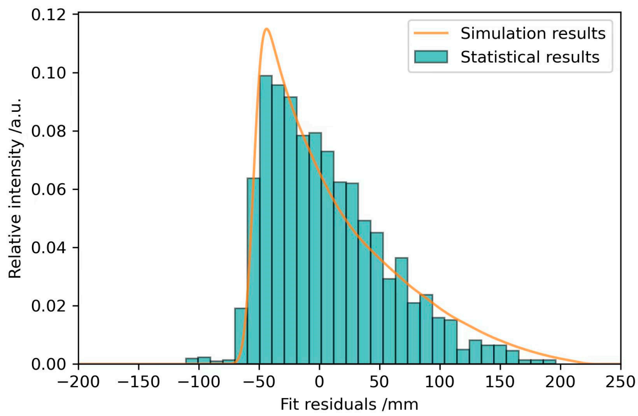

Figure 4. Distribution of the returned signals from Etalon at different incident angles. The orange curve corresponds to the simulated echo signal based on the retroreflector uneven distribution model.

3. Pre-Processing Algorithm with a Center of Mass Corrections Filter

A normal point algorithm is a universal method applied in the pro-processing of SLR raw observation data [13]. It eliminates the noise point by a Poisson statistical filter and polynomial filter. Specifically, the first step involves fitting a trend function to the raw range or the residuals from a predicted orbit in order to remove all signatures from the orbit, and then analyzing the distribution of the trend-removed data. In order for a trend function to be fitted iteratively, some level of screening must be performed. Letts criterion method recommends an iterated 2.5 $\times$ rms rejection criterion for signal photon detection SLR systems and an iterated 3 $\times$ rms rejection criterion for multi-photon level detection systems. A fitting residual is the deviation of each observation point from the fitting function, which is approximately equal to the random error of the observation point.

It Is noteworthy that If these data have a symmetrical distribution about the peak, using the 2.5 $\times$ rms rejection criterion should be acceptable. However, if the data have a skew distribution, then the arithmetic mean will be biased away from the peak, and the amount of bias will probably depend on the level of final screening applied. The 2.5 $\times$ RMS screening may not be appropriate for skew distributions of observational data.

We simulate the echo signals returned by Etalon from all directions and extract the effective echo signals using the normal point algorithm. The relationship between the center of mass corrections and the incident angles is illustrated in Figure 5.

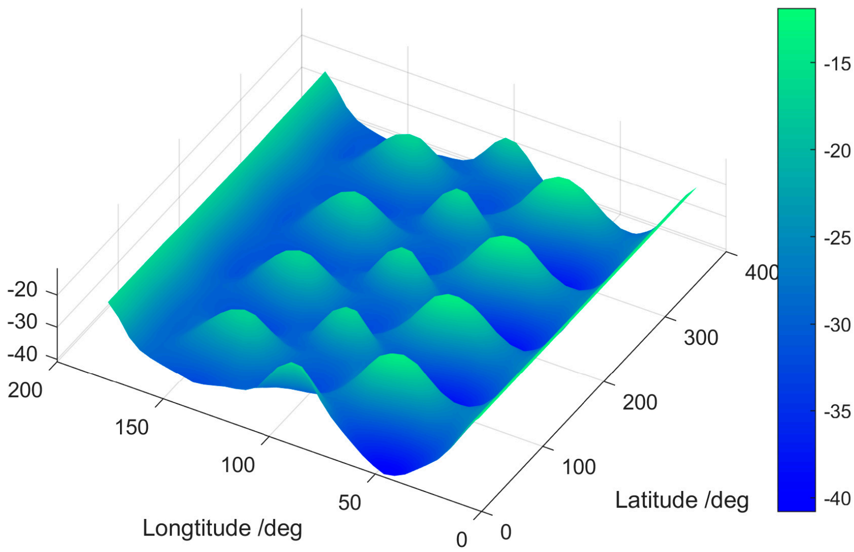

Figure 5. Variation of the center of mass corrections with incident angles.

Even though the normal point algorithm is used to process the raw data from Etalon, the center of mass corrections at different incident angles are not stable. The center of mass corrections will increase when the incident beam is irradiated to an area densely covered by the reflectors, and vice versa. The calibrated results reveal a mean value of 572.5 mm for Etalon's center of mass corrections, which is almost identical to the value offered by the ILRS [14]. As a result of the different orientations of the satellites, the range of the Etalon center of mass corrections has shifted by 28 mm, from 558.8 mm to 586.8 mm. Additionally, we calibrated the root mean square roughness (RMS) of the center of mass corrections for various incident angles. There is a high RMS of 6.7 mm, as demonstrated by the results. The data presented here support the notion that variations in the center of mass corrections for Etalon are responsible for additional range bias in the measurements.

In order to eliminate the range bias introduced by the variable effect in the center of mass corrections, we analyze the relationship between the acceptable level for normal point formation and the RMS of center of mass corrections. The 2.5 × RMS noise filtering is modified as:

$$p(x) = \begin{cases} p_{FR}(x)\,, & \text{if} -2.5 \times \sigma \le x \le r \\ 0\,, & \text{else} \end{cases}, \tag{5}$$

where r is the set limit to clip the full-rate observation data. The range residuals are selected and clipped from $-2.5 \times$ RMS to r to form and calibrate the center of mass corrections. The RMS of the center of mass corrections is the result of 2594 reflected signals for the incident directions equally distributed around Etalon. We quantify the association between clipping location and mean square error (RMS) of center of mass, shown in Figure 5.

Figure 6 illustrates that the clipping location has a significant impact on the RMS of the center of mass corrections. With the increasing of r, the mean RMS of center of mass corrections gradually decreases, then rises, and finally settles. Variations in the RMS of center of mass can be explained by the acceptance level of range residuals for normal points. By r setting to 3.34 mm, the RMS of center of mass corrections will be minimized, which means the range error introduced by the variation of the satellite signature effect will be reduced to a minimum.

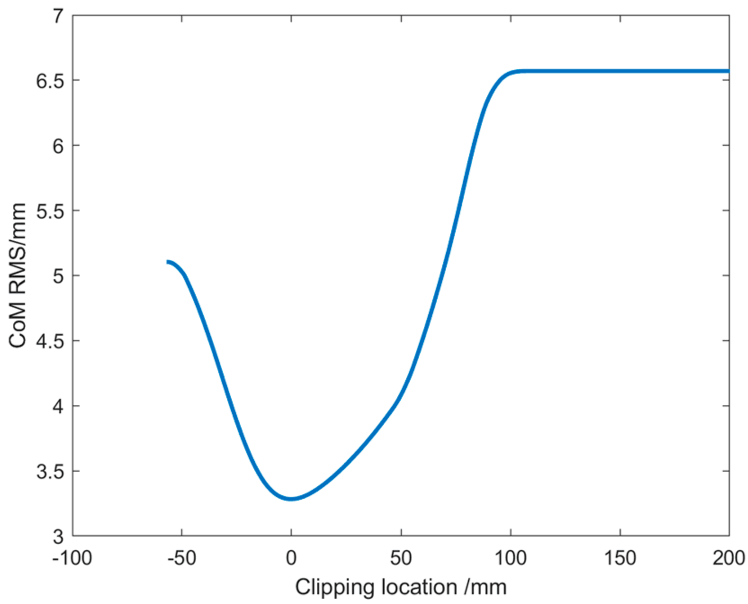

Figure 6. Relationship between RMS of CoM and clipping location of the range residual distribution for normal points.

We propose a center of mass corrections filter that is applied to the normal point algorithm in order to correct for satellite signature effect on SLR data. In the suggested method, the residual histogram is located first by using a least-squares approach. Afterwards, residuals from the selected range are clipped with a $-2.5 \times$ RMSrange in order to remove the noise points caused by the satellite signature effect. The selected residuals are then clipped by the second clipping step using $2.5 \times$ RMS criteria to form the SLR production. A flowchart of the SLR post-processing algorithm with a center of mass corrections filter is shown in Figure 7.

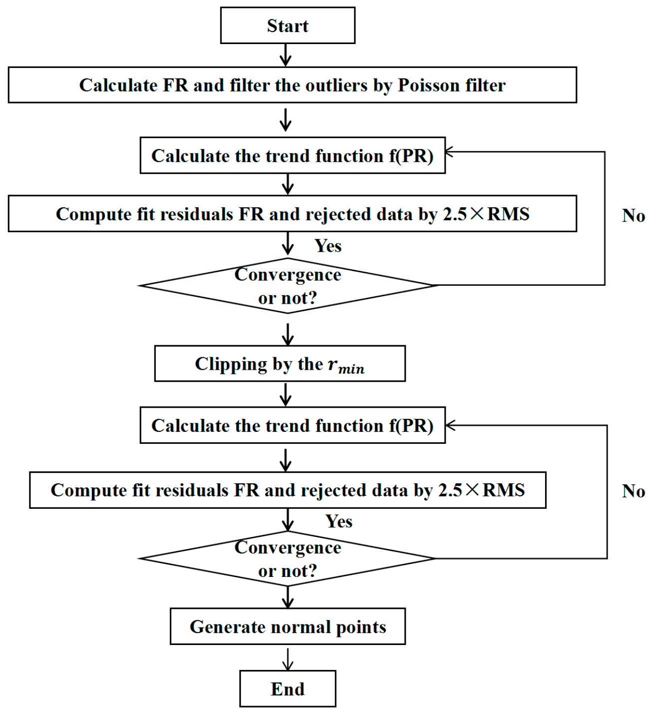

Figure 7. The diagram of the new proposed SLR algorithm.

4. Discussion

Based on one month of kHz SLR passes of Etalon-1 collected by the Changchun observatory, we demonstrate that the new method provides different results from the previous method. Figure 8 illustrates the processed observation data for the period from 1 January to 26 January in 2022. The RMS for each normal point processed by the new proposed algorithm is significantly reduced. In addition, the kurtosis as well as skewness for the observed distribution in actual residuals are smaller, as well. It is important to note that the noise signals originating from the tails of post-fit range residual distributions are eliminated, as a result the residual waveform, is more similar to that of a normal distribution. An improvement in the quality of the SLR data collected by the observatory has been demonstrated with the introduction of the center of mass corrections filter.

In order to verify the applicability of this new algorithm, we also analyze Etalon-2 observation data with the same procedures, as shown in Figure 9. Based on the results of the analysis, Etalon-2 observation data processed by the new algorithm show superior accuracy and stability in comparison to Etalon-1 observation data.

In Table 1, we summarize the statistical observations related to Etalon-1/2 processed via these two methods. Compared to the results calibrated with the normal point algorithm, the new algorithm with the center of mass corrections filter has a better performance. For Etalon-1, the average RMS per normal point (NP) is decreased from 163.7 $\pm$ 41.8 ps to 118.2 $\pm$ 8.94 ps while the stability of normal point is improved by 79%. As for Etalon-2, the average RMS per NP is reduced from 145.4 $\pm$ 34.3 ps to 120 $\pm$ 7.47 ps, while the stability of normal point is improved by 78%. Both kurtosis and skewness per NP are significantly reduced, which indicates that satellite signature effect has a minimal impact on temporal spread. It can be believed that the new processed observation data are more stable and reliable.

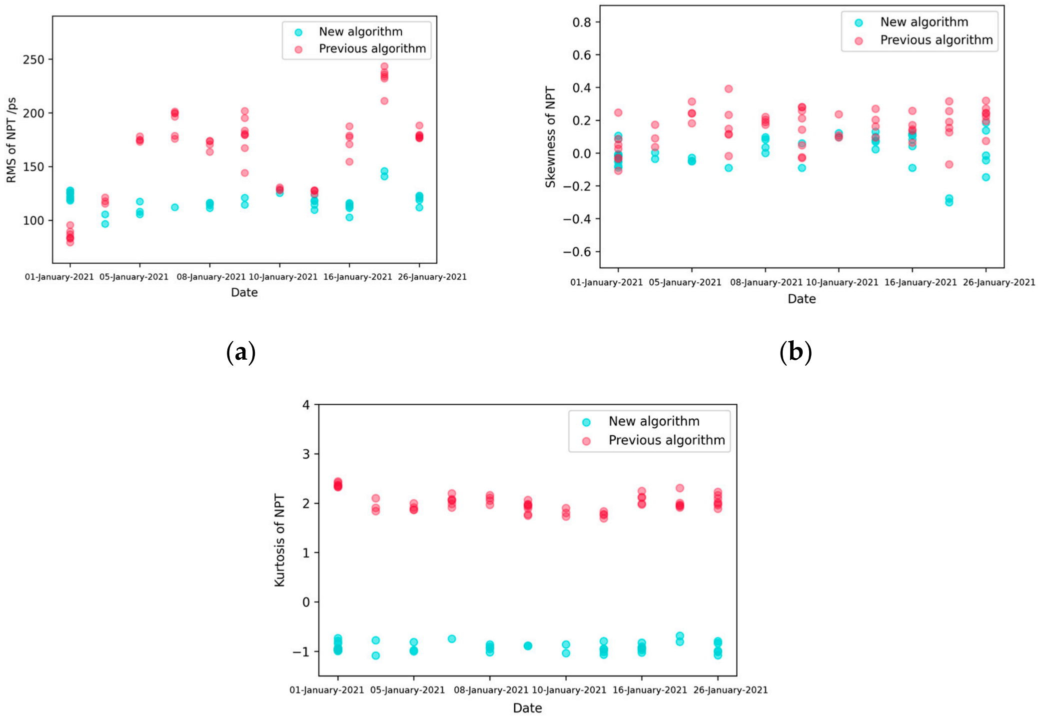

(**a**) (**b**)

(**c**)

Figure 8. Etalon-1 satellite data processing results (**a**) RMS of NPT, (**b**) skewness of NPT, (**c**) kurtosis of NPT.

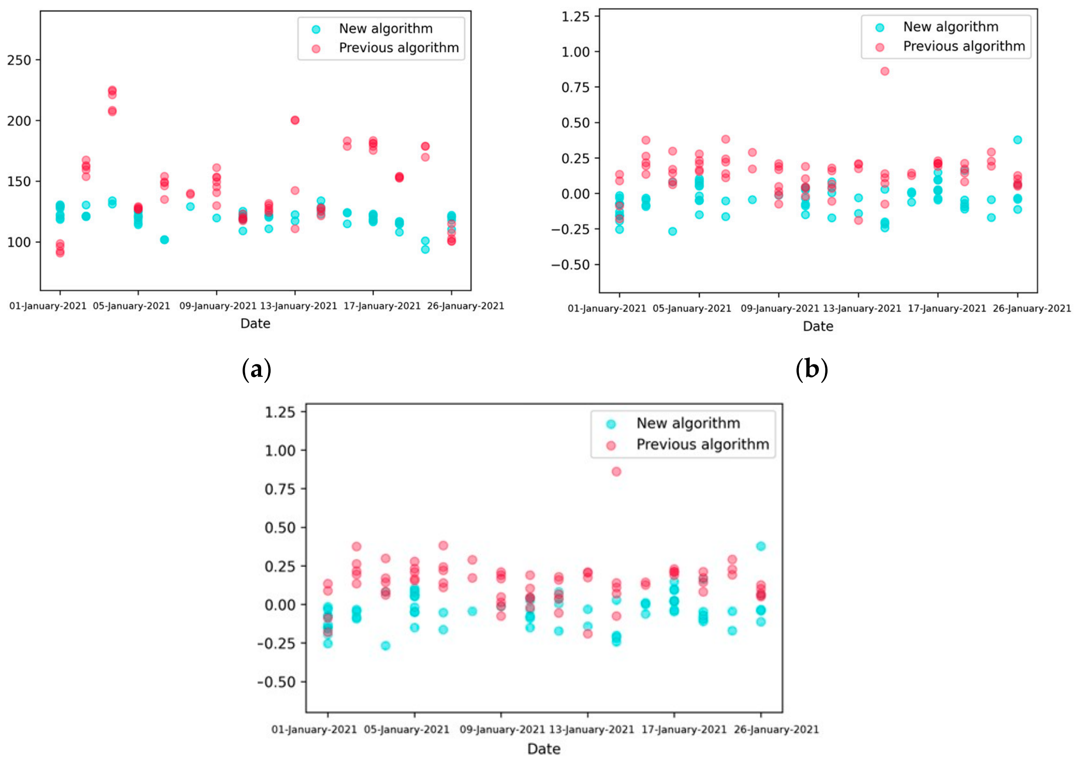

(**a**) (**b**)

(**c**)

Figure 9. Etalon-2 satellite data processing results (**a**) RMS of NPT, (**b**) skewness of NPT, (**c**) kurtosis of NPT.

Table 1. SLR observation characteristics of Etalon satellites.

	Etalon-1			Etalon-2		
	RMS (ps)	**Kurtosis**	**Skewness**	**RMS (ps)**	**Kurtosis**	**Skewness**
Normal point algorithm	163.7 ± 41.8	−0.91 ± 0.1	0.16 ± 0.1	145.4 ± 34.3	1.96 ± 0.2	0.15 ± 0.14
New proposed algorithm	118.2 ± 8.94	2.02 ± 0.18	0.01 ±0.1	120 ± 7.47	−0.95 ± 0.12	−0.04 ± 0.1

As a further verification of the efficacy of the new proposed SLR processing algorithm, Etalon-1/2's external precision is calibrated using the precise satellite ephemeris SP3 of the International GNSS Service (IGS). Figure 10 illustrates the residual distribution of Etalon-1/2 computed using the two approaches outlined above.

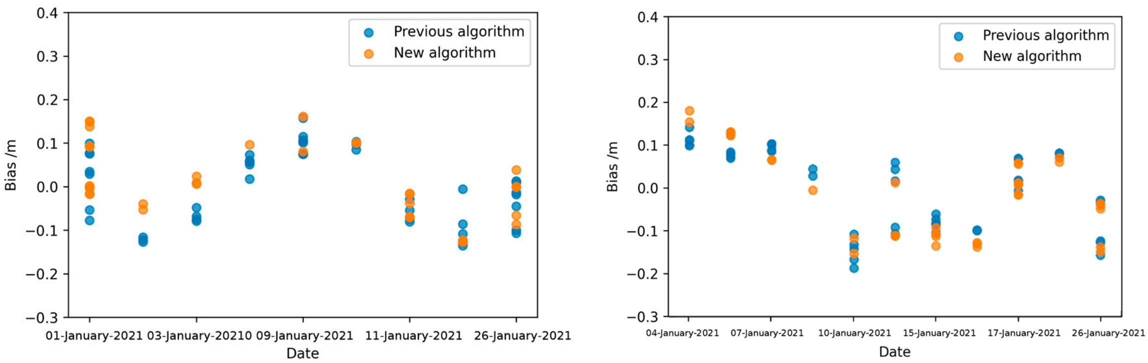

(**a**) (**b**)

Figure 10. Residual distribution of Etalon-1/2 processed by different SLR algorithms: (**a**) Etalon-1; (**b**) Etalon-2.

The calibrated results indicate that the external precision of Etalon-1 normal points processed by the new algorithm has been reduced from 8.4 cm to 7.5 cm. By introducing the center of mass corrections filter, the external precision of Etalon-1 satellite observation results has been improved by 0.9 cm. However, it was not successful on Etalon-2. RMS of the residuals obtained by the standard point algorithm for Etalon-2 normal points is 9.4 cm, while RMS of the residuals obtained by the new algorithm is 9.7 cm. A possible explanation may be the small number of Etalon satellite observation points or the long observation interval.

5. Conclusions

Etalon is one of the most important geodetic satellites, which is responsible for a wide range of scientific research and observation activities. Due to its spherical shape and optical properties of retroreflectors, Etalon is susceptible to the effects of satellite signatures on laser ranging. A numerical simulation of the satellite signature effect on Etalon signals is carried out by using an uneven distribution model for retroreflectors. It has been demonstrated by the data collected from the kHz SLR system in Changchun that the average residual distribution of simulated returns is consistent. By processing the simulated signals via the standard algorithm, the center of mass corrections for Etalon are found to be shifted from 558.8 to 586.8 mm at various incident angles. Based on this evidence, it seems that the standard procedures for SLR data cannot minimize the effect of range bias caused by deviations in the center of mass corrections..

For further reduction of satellite signature effects on ranging data, a center of mass correction filter is applied as part of the standard post-processing of Etalon observations. The range measurements with the lowest RMS of center of mass corrections are selected for the formation of normal points. Statistical analysis of the results demonstrates that a reduction in the average RMS of normal points per pass is from 163.7 ± 41.8 ps to 118.2 ± 8.94 ps, while the stability of normal points is improved by 79%. It is evident from the distribution of returned signals that are processed via the new algorithm that the distribution is more concentric and stable with smaller kurtosis and skewness per NP. Additionally, we applied the new algorithm into the post-processing for Etalon-2, which improved the ranging accuracy and stability of the normal points. A theoretical reference is provided in this study, which identifies previously unrecognized errors in the observation and provides a practical approach to further enhance its quality.

It is admitted that the present study cannot be used for all satellites, but only for sphere satellites with significant satellite signature effects on echo signals. In contrast to satellites with a flat-plate structure, satellites with a flat-plate structure do not have any problems related to variations in satellite signature effects caused by varying incident angles.

Author Contributions: Conceptualization, N.A. and B.G.; methodology, J.G.; formal analysis, N.E.N.; investigation, R.C.P.; writing—original draft preparation, N.A.; writing—review and editing, X.D.; software, H.Z. and B.G.; funding acquisition, N.A. All authors have read and agreed to the published version of the manuscript.

Funding: This research was funded by National Natural Science Foundation of China, grant number 12073052 and 11973064, Jilin Province Science and technology development program, grant number 20230101006JC, Chinese Academy of Sciences International Talent Program, grant number 2024VIMA0009.

Data Availability Statement: The data presented in this study are openly available.

Conflicts of Interest: The authors declare no conflict of interest.

Appendix A

The SLR system diagram in Changchun station are as followed:

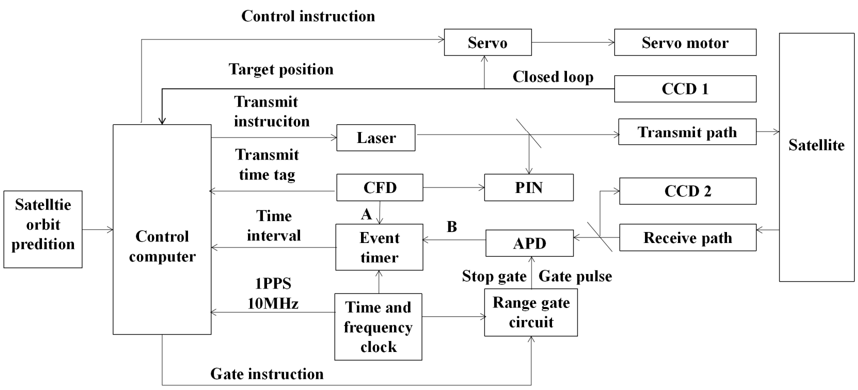

Figure A1. Changchun SLR system diagram.

References

1. Kucharski, D.; Kirchner, G. Spin parameters of High Earth Orbiting satellites Etalon-1 and Etalon-2 determined from kHz Satellite Laser Ranging data. *Adv. Space Res.* **2014**, *54*, 2309–2317. [CrossRef]
2. Lian, L.-Z.; Wang, J.-X. Weekly inter-technique combination of SLR, VLBI, GPS and DORIS at the solution level. *Res. Astron. Astrophys.* **2018**, *18*, 119. [CrossRef]
3. Mathis Bloßfeld, S.R.; Alexander, K. Consistent estimation of geodetic parameters from SLR satellite constellation measurements. *J. Geod.* **2018**, *92*, 19. [CrossRef]
4. Ibrahim, M.; Abd El-Hameed, A.M. Analytical investigation for the satellite ranging data of changchun SLR station. *NRIAG J. Astron. Geophys.* **2020**, *9*, 321–329. [CrossRef]
5. Guan, B.; Fan, C. A SLR Pre-Processing Algorithm Based on Satellite Signature Effect. *Appl. Sci.* **2021**, *11*, 8880. [CrossRef]
6. Strugarek, D.; Sośnica, K. Detector-specific issues in Satellite Laser Ranging to Swarm-A/B/C satellites. *Measurement* **2021**, *182*, 109786. [CrossRef]

7. Kirchner, G.; Franz, K. Millimeter Ranging to Centimeter Targets. In Proceedings of the 16th International Workshop on Laser Ranging, Poznan, Poland, 13–17 October 2008.
8. Kucharski, D.; Kirchner, G. A method to calculate zero-signature satellite laser ranging normal points for millimeter geodesy-a case study with Ajisai. *Earth Planets Space* **2015**, *67*, 34. [CrossRef]
9. Wilkinson, M.; Schreiber, U. The next generation of satellite laser ranging systems. *J. Geod.* **2018**, *93*, 2227–2247. [CrossRef]
10. Pearlman, M.; Arnold, D. Laser geodetic satellites: A high-accuracy scientific tool. *J. Geod.* **2019**, *93*, 2181–2194. [CrossRef]
11. Rodríguez, J.; Appleby, G. Upgraded modelling for the determination of centre of mass corrections of geodetic SLR satellites: Impact on key parameters of the terrestrial reference frame. *J. Geod.* **2019**, *93*, 2553–2568. [CrossRef]
12. Otsubo, T.; Appleby, G.M. System-dependent center-of-mass corrections for spherical geodetic satellites. *J. Geophys. Res. Solid Earth* **2003**, *108*, 1–9. [CrossRef]
13. Otsubo, T.; Sherwood, R.A. Center-of-mass corrections for sub-cm-precision laser-ranging targets: Starlette, Stella and LARES. *J. Geod.* **2014**, *89*, 303–312. [CrossRef]
14. Herrera Pinzon, I.; Rothacher, M. Differencing strategies for SLR observations at the Wettzell observatory. *J. Geod.* **2022**, *96*, 4. [CrossRef] [PubMed]